This is a preprint of the accepted conference paper:

Spröwitz, Alexander, Chantal Göttler, Ayush Sinha, Corentin Caer, Ugur Mehmet Ötzekin, Kirstin Petersen, and Metin Sitti. “**Scalable Pneumatic and Tendon Driven Robotic Joint Inspired by Jumping Spiders**.” In Proceedings of IEEE International Conference on Robotics and Automation (ICRA), 64–70, 2017.

@inproceedings{sprowitz_icra_2017,
	title = {Scalable {Pneumatic} and {Tendon} {Driven} {Robotic} {Joint} {Inspired} by {Jumping} {Spiders}},
	booktitle = {Proceedings of {IEEE} {International} {Conference} on {Robotics} and {Automation} ({ICRA})},
	author = {Spr\”owitz, Alexander and G\”ottler, Chantal and Sinha, Ayush and Caer, Corentin and \”Otzekin, Ugur Mehmet and Petersen, Kirstin and Sitti, Metin},
	year = {2017},
	pages = {64--70}
}

Scalable Pneumatic and Tendon Driven Robotic Joint Inspired by Jumping Spiders

Alexander Spröwitz[1], Chantal Göttler[1], Ayush Sinha[2], Corentin Caer[3], Mehmet Uğur Öztekin[4], Kirstin Petersen[5], and Metin Sitti[1]

***Abstract*— Fluidic actuators allow versatile, agile, and powerful motions and are commonly applied in robotics and automation. Likewise, many biological systems use fluidic actuators implemented with tissue for a wealth of tasks and performances. Spiders for example apply a hybrid mechanism of hydraulically actuated joint extension and muscle-based joint flexion to produce movement in two of their seven leg joints. Here, we present a novel spider-inspired joint mechanism employing both pneumatics and electrically-actuated tendons capable of strong, dynamic, and rapid joint movement. The implementation of the joint is closely inspired by those seen in real spiders, with a foldable structured membrane that effectively transfers all the energy from pressure to torque as the leg unfolds. To evaluate the mechanism we derived static joint models and a simple jumping model, and conducted equivalent experimental tests with a prototype of a single jumping leg robot. Besides applications in robot locomotion, the implementation and modeling of the spider-inspired joint mechanism can be utilized to further explore dynamics and functional biomechanics in spiders. In the future, we hope to use this platform to answer questions related to the impressive jumping and locomotion performances of real arachnids, and explore what morphological traits lie behind efficient spider locomotion at different size scales.**

I. Introduction

Arachnids are a highly successful species, numbering over 100 000 species and found in all climates and areas of specialization, including social and solitary individuals living in webs, burrows, on and even under water surfaces. Spiders, for example, span more than 100 times in size. Jumping spiders are on the millimeter-scale, whereas the giant huntsman spider [1] scales up to 30 cm. Their role as predators and prey have spurred a wealth of locomotion strategies; they may run on land and water, jump large distances, navigate complicated vertical surfaces and delicate webs, and some even raise their front legs in an attempt to imitate the look of antennae on ants [2], [3]. It is therefore no surprise that they have served as loose inspiration to a great number of robots both as toys and scientific platforms [4], [5]. Here, we take a closer look at the inner workings of spider leg joints, designing a corresponding mechanical mechanism and demonstrating its use in a jumping robot leg.

[1]Max Planck Institute for Intelligent Systems, 70569 Stuttgart, Germany, and Max Planck ETH Center for Learning Systems [sprowitz, goettler, sitti]@is.mpg.de
[2]Indian Institute of Technology, Kanpur, India 208016 ayushs@iitk.ac.in
[3]Horace Mann School, NY 10471, USA tino.caer@me.com
[4]Middle East Technical University, Turkey m.ugur.oztekin@gmail.com
[5]Cornell University, NY 14853, USA kirstin@cornell.edu
*Chantal Göttler was funded by the Max Planck ETH Center for Learning Systems.

II. Related Work

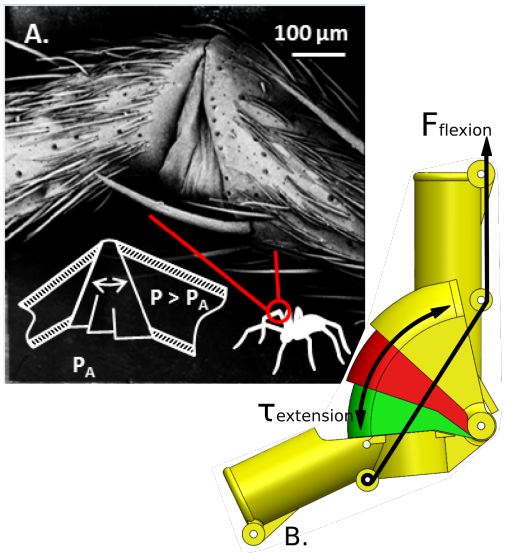

Fig. 1: Concept behind the spider-inspired leg joint using hybrid actuation. **A.** Scanning electron microscope image of the tibia-metatarsus joint of a wolf spider (*Trochosa* spec.), lateral view. The insert shows a stylized version of the bellow-like structure of the exoskeleton, also mentioned in [6]. **B.** CAD drawing of robotic joint inspired by the spider-joint. Torque τ from internal fluid (air) pressure is applied to extend the joint, and cable force F flexes the joint.

Arachnids have exoskeletons and locomote and interact with their environment with the help of hybrid joint actuation. Interestingly, two of its seven leg joints (femur-patella and tibia-metatarsus) lack extensor muscles, i.e. the ability to stretch those joints through direct muscle force [7]. Instead, researchers have found that spiders create blood ("haemolymph") pressures within their legs to stretch those joints, and use flexor muscles to bend them. Although this theory was first presented in 1957 [7], and has been supported many times since [6], [8], [9], researchers still argue over how this pressure is generated and augmented, and whether it is indeed the primary force of locomotion in larger spiders [10]. The benefit of a central (located in the spider's prosome) hydraulic system is that the majority of mass is located proximally, minimizing the inertial forces

when the long legs move. Unfortunately, it also precludes prolonged vigorous activity [8]. As spiders increase in size it takes longer to build up the pressure in their legs; reversely smaller spiders are potentially limited by the flow impedance of narrow veins [11]. The overarching goal of this work is not just to enable more versatile robots, but, more importantly, also to start establishing a feasible model with which we may advance our understanding of the hybrid joint actuation in spiders.

Several researchers have presented spider-inspired mechanisms. Early works involved preliminary design concepts for hydraulic devices [6], [12] and flexible joints for medical and robotic applications [13]–[16]. These were all focused on hydraulics or pneumatics only, and did not include the combined use of pressure based joint extension and cables to flex the joint. Notable recent work comprise a four-bar linkage system with a tendon-controlled spring-loaded joint for front-leg assisted targeted jumping [17]. In contrast to prior work, the mechanism presented here combines a pressurized joint with a flexor tendon, and has a folding bellow-like design reminiscent of the real spider leg, see Fig. 1. To ease the fabrication process, the mechanism is multiple times larger than its biological counterpart; to lower the weight, simplify fabrication, and increase the jumping height we use air instead of liquid inside in the joint. However, the design principles shown should work on many different size scales with a variety of (low viscosity) fluids.

In this paper we present the design of joint and tendon mechanisms, static characterization of the joint embedded into a single leg, and dynamic characterization of an one-legged platform capable of jumping. Jumping is a popular form of locomotion for robots, allowing them to traverse unstructured terrain while gaining good visual perspective from above. Correspondingly, researchers have tackled this problem in many different ways, ranging from spring-loaded mechanisms [18], [19] and pneumatic pistons [20], to soft robots powered by explosions [21]. Additionally, an impressive spider-scale jumping robot was presented in 2008 [22], using material buckling instabilities to rapidly jump on the surface of water. Although we are not able to demonstrate jumps as impressive as some of these other robots, we do present a simple, low weight mechanism with proximally located bulk mass, which is closely related to the hybrid joint actuation of real spiders. This approach has many advantages: 1) it works across different size scales, 2) it has a leg joint torque source with mostly linear torque-pressure characteristics, and 3) a single driver mechanism may be used for one as well as multiple joints with only small modifications.

III. Mechanical and Experimental Design

In this section we describe the mechanical design of the spider-inspired leg joint, its flex-hold-release mechanism, and the static and dynamic experimental characterization setup.

Mechanical joint design: Spider leg joints appear to have a foldable membrane structure (Figure. 1a) that allows the leg to rotate and produce torque when actuated through haemolymph pressure [6]. The specific design of this membrane is critical to translate maximum energy from pressure to torque in the joint, yet the details of how they develop and maintain their functionality remain unknown.

In an optimal design, the membrane keeps its contact angle (CA, Fig. 3) mostly perpendicular to the pressure active chamber area, A (Fig. 3c). Deviation from a perpendicular CA (Fig. 3d) creates force components of smaller amplitude; a perpendicular $F_{\perp}$ and a parallel $F_{\parallel}$. This reduces joint torque production and might even counter extension torque. A CA $> 90°$ [6] is especially pronounced in soft, unrestricted membranes that tend to bulge outwards (Fig. 3d). Bulging creates a parasitic volume V_{bulge} which requires energy and time to fill. The volume of the bulge follows a nonlinear (quadratic) radius-volume relation leading to high losses, which subtracts from the pressure generating torque within the active volume V_{active} (see also Eqn. 4).

Inspired by scanning electron microscope (SEM) pictures and close-up photos of spider joints (Fig. 1 and [3]), we explore the idea of a joint with perpendicular CAs through multiple stacked, rigid shell elements with an internal, sealed membrane (Fig. 2, Fig. 4b). In the flexed leg posture, shell elements are stacked within each other. During joint extension, shell elements extend in a rotatory fashion (Fig. 5). The shape of the shell elements follows a perpendicular CA and limits the internal pressurized bag to the same shape (Fig. 1, Fig. 2, Fig. 4b).

We tested several materials for the internal bag which seals the air in the actuator joint. Latex balloons have the advantage of adapting well to uneven shell shapes. When pressurized, however, large friction between the internal bag and the shell elements prevented dynamic and fast leg extension. Instead, we settled on custom-made low-friction thermo-bonded freezer storage bags (Fig. 4b). A custom-made plug seals the connection between the tube and the internal bags. Leg segments, pressure volume, and leg shell elements are 3D printed in VeroClear (Stratasys Objet 226). Leg and shell elements are connected via small metal pins of $1.6\,\text{mm}$ diameter.

The implemented leg has two leg segments with a length of $70\,\text{mm}$, a diameter of $15\,\text{mm}$, and a wall thickness of

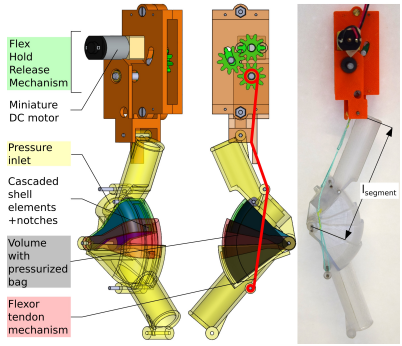

Fig. 2: CAD drawings and image of real leg joint, emphasizing functional components. The overall weight of the system is $36\,\text{g}$, the ground to hip height in the flexed state is $105\,\text{mm}$, at a leg segment length of $70\,\text{mm}$.

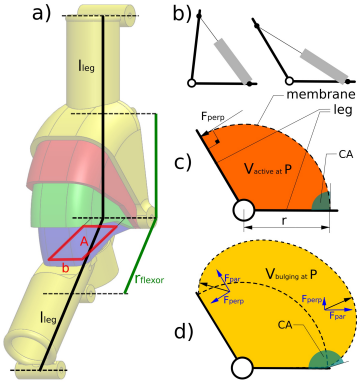

Fig. 3: a) and c) Geometric parameters: b width of shell segments, r height of shell segments, A pressure area, p pressure within the chamber, r_{flexor} flexor tendon lever. b) Schematic drawing of leg joint actuated by a telescopic actuator: a linear change in actuator length leads to a nonlinear/cosine change of joint angle. c) If the contact angle (CA, green) between membrane and active area is perpendicular, all pressure vectors contribute fully to joint extension. d) Especially in soft membrane actuators the membrane tends to bulge and CA $>90°$. Pressure vectors located at the rim between active area and membrane, and pressure vector components applying force to the membrane will lead to parasitic forces lowering the joint extension torque. Further, a large volume V_{bulging} must be filled and pressurized, at the additional cost of energy and time.

1.5 mm. The three moving shell elements (Fig. 5, blue, green, and red) have an external height of radius r 24 mm, 25.5 mm and 27 mm, an external width b of 15.5 mm, 17 mm, and 18.5 mm, and a center axis of radius $c = 3$ mm, leading to a maximum active area of $A_1 = (r-c)\times b = 444\,\text{mm}^2$ (Fig. 5). The total weight of the two leg segments, connector pins, internal bag, and shell elements is 14 g. The assembly of the internal bag, connector, and chamber segments weigh ≈ 4 g, corresponding to 11 % of the weight of the leg mechanism. A reservoir volume of $V_{\text{reservoir}} \approx 12\,000\,\text{mm}^3$ between pump and active leg volume consisted of the interconnecting silicone rubber tubes and a small extra, reservoir volume. The externally mounted miniature air pump has a weight of 14 g, and produces between 55 kPa and 58 kPa maximum gauge pressure, at 98.5 kPa ambient air pressure. The maximum rotational working range of the implemented leg is $3\times 23° = 69°$.

Flexing and release mechanism: The second part of the hybrid, spider-inspired joint concerns the instantaneous power a spider can produce to jump. Muscles have instantaneous force and velocity characteristics that might limit jumping performance. Alternatively, the integration and slow build-up of energy through a charging mechanism is plausible; leg joints are flexed and held by muscle force, then pressure is increased at fixed joint posture until eventually the joint is rapidly released by relaxing flexor muscles. In our setup the flexor muscle is replaced by a flex-hold-release cable-driven mechanism actuated by an onboard miniature DC motor (Fig. 2). This flex-hold-release mechanism is inspired by the Dash crawler clutch mechanism [23]. We initially implemented a cam-based mechanism similar to [18]. However, the fixed charging and release range limited the leg design, and added complexity and weight. The finally implemented flex-hold-release mechanism including a 300 : 1 geared DC motor of 10 g comprised ≈ 60 % of the total weight of the leg mechanism.

Static and dynamic experiments: We characterized the joint in a static setup by recording simultaneous data of the internal chamber pressure, external joint torque, and leg joint angle (Fig. 4a). Initially, the leg joint was flexed and held against a load cell, with the internal bag at ambient air pressure. The chamber was then connected to a miniature air pump through a 3 mm diameter silicone tube and a small reservoir volume. The pump motor worked at 3 V and an average of 0.3 A for 10 s to increase the maximum gauge pressure of 58 kPa. The leg was slowly released (quasi-static test), typically within a 3 s to 5 s time window. Torque was measured by a 5 kg, single-axis load cell connected to a Buster 9236-V100 strain gauge supply and amplifier. Analog output data was read in a National Instruments NI USB-6363 data acquisition board at 1 kHz, through a custom LabVIEW interface. Chamber pressure was measured with a Phidget 1140 pressure sensor, its output data was processed through the National Instruments acquisition board and the LabVIEW interface. Leg joint positions were obtained with a Sony camcorder camera at 30 Hz, by recording colored markers on the leg joint and extracting marker positions with Physlets Tracker software. Pressure and torque data was automatically synchronized through the common LabVIEW interface, video data was synchronized by a modest tap against the load cell. All data was processed in Matlab; outliers such as from initially tapping the force sensor were removed manually. Next, the joint was dynamically characterized by a simple, free vertical jump. The leg was placed in a vertical position against a holder, the air pressure tube and a small reservoir volume were connected to the air pump, and the flex-hold-release mechanism was connected to an external power supply. The jumping movement was recorded with a high-speed camera model Phantom V461 at 1 kHz. Electrical supply cables for the release motor and the pressure tube

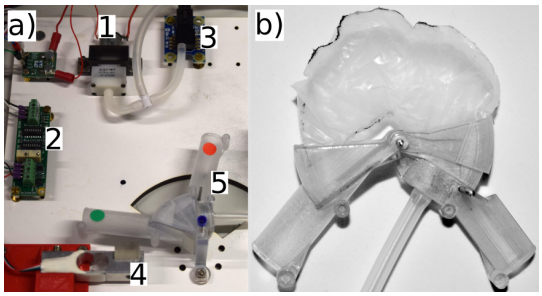

Fig. 4: a) Setup to characterize the static torque-pressure-angle characteristics of the spider-inspired joint: 1 miniature air pump, 2 Wheatstone bridge supply and ADC, 3 pressure sensor, 4 force sensor, 5 spider-inspired robot joint. b) Robot leg with shell elements removed to show the internal custom-made pressure bag. Without the mechanical restraints of its shell elements, the pressure bag bulges outwards and extends largely beyond the optimal shape.

were placed to hang loosely on the leg, and not hinder the jump. The motor was engaged to flex the leg joint through the tendon cable mechanism (see Fig. 2 and video in supplementary material) until the motor stalled. Air pump pressure was applied between 7 s and 10 s. Immediately after the onboard motor was activated rapidly releasing the joint-flexing cable. Jumping height based on the robot's approximate center of mass at hip height, and working angle α defined as the change of angular leg joint angle during ground contact were extracted from the high speed video footage.

IV. Characterization and Modeling

In order to characterize the spider-inspired joint we *a)* modeled extension torque based on working angle and chamber pressure, and *b)* potential jumping height based on positive work releasing the air-spring, and working angle. We compare modeled values with the experimentally obtained data in a static and a dynamic testing setup.

Static Joint Torque Model: Here we show how torque develops as a function of pressure and angle, within the active volume of the joint. After switching off the external pump, pressure $p(\alpha)$ changes as a function of joint angle with the consecutive opening of the shell segments (Fig. 5). Torque $\tau(\alpha)$ is a result of force acting perpendicular ($F_\perp$) onto the center of the active pressure area $A_{\text{active}} = (r(\alpha) - c) \cdot b(\alpha)$ at a lever length of $\frac{1}{2}(r(\alpha) + c)$ of the active chamber, with c as the radius of the joint axis (Fig. 3a). Width $b(\alpha)$ and height $r(\alpha)$ of the active area vary with the consecutive opening of each shell element. The acting force $F_\perp$ is a direct result of chamber pressure $p(\alpha)$ applied at the active area A_{active}:

$$F_\perp(\alpha) = p(\alpha) \cdot A_{\text{active}} \quad (1)$$

$$\tau(\alpha) = F_\perp \cdot 1/2 \cdot (r(\alpha) + c) \quad (2)$$

$$\tau(\alpha) = 1/2 \cdot p(\alpha) \cdot b(\alpha) \cdot (r(\alpha)^2 - c^2) \quad (3)$$

Eqn. 3 shows that width b of the active chamber contributes linearly to the output torque. Torque depends linearly on instantaneous pressure $p(\alpha)$. Pressure is reduced stepwise due to stepwise change of volume, but is majorly governed by the working angle α. Importantly, height r of the pressure chamber contributes quadratically to the torque, and small variations of r lead to large changes in output torque. This comes at a quadratic cost for chamber height r contributing to the active chamber volume:

$$V(\alpha) = \frac{\alpha}{2\pi} \cdot b(\alpha) \cdot r(\alpha)^2 \cdot \pi \quad (4)$$

Both the volume and the active area change stepwise when switching between shell elements, according to Fig. 5. The resulting pressure p can be estimated via the initial pressure, and the change of the sum of volumes $V = V_{\text{active}}(\alpha) + V_{\text{reservoir}}$. The pressure-volume relationship depends on the assumed model; $\gamma = 1$ for an isothermal model; and $\gamma = 7/5$ for an adiabatic model assuming air as a diatomic gas:

$$p(\alpha) = p_{\text{init}} \cdot V_{\text{init}}^{\gamma} \cdot \frac{1}{V^{\gamma}(\alpha)} \quad (5)$$

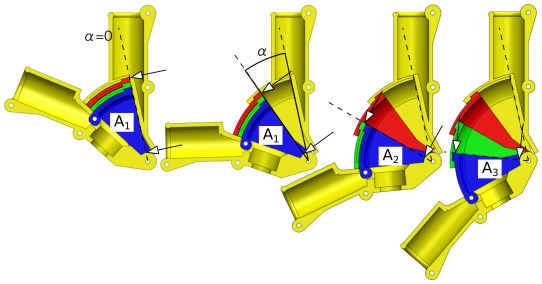

Fig. 5: Opening sequence of shell elements. Also observed in high speed recordings, joint segments start opening with the largest to smallest segment: red first, then green, then blue. This leads to a sequential, non-continuous change of the pressure-active area A_{active} (between white arrow heads) from the largest area A_1 to the smallest area A_3. The active volume changes accordingly in a non-continuous fashion. Working angle α and its zero reference are indicated.

Both models show a stepped torque response to a changing pressure or the related working angle, visible in the jagged-line plots of Fig. 6 and Fig. 7. We assume the isothermal model is more valid for experiments with sufficient time and surface area to settle the temperature difference between chamber and environment, such as for static experiments and its data shown in Fig. 6 and Fig. 7. For fast movements like the jumping experiments and no time to adapt chamber temperature to outside temperature, we assume a more adiabatic behaviour including a temperature drop through rapid volume expansion.

The difference between the isothermal and the adiabatic model is significant in this application example: the adiabatic model drops pressure and torque faster compared to the isothermal model. This results in zero gauge pressure at $\alpha = 40°$, and the chamber pressure becomes equal to the outside, atmospheric pressure. Theoretically, a further increase of the joint angle at the adiabatic model assumption would reduce the chamber pressure below external atmospheric pressure, and the internal bag would start deflating. However, the pressure bag produces only compressive forces and detaches from the walls once its internal pressure equals the outside pressure. The torque-pressure plot (Fig. 6) indicates a piecewise linear behaviour of both the isothermal and the adiabatic model in the plotted pressure range. Vertical steps follow the abrupt changes between shell segments. The isothermal model shows at $\alpha = 40°$ still $0.1\,\text{Nm}$ remaining joint torque. The isothermal model expands the leg joint up to $69°$ (Fig. 7), $29°$ more than the adiabatic model.

Static Experimental Joint Characterization: Experimental, static measurements included sensor values of force (torque) and pressure, which where synchronized to the measurements of the working angle (setup Fig. 4). Experimental torque values are plotted as a function of joint pressure (Fig. 6), and are compared to the adiabatic-model and isothermal-model torque (Eqn. 3 and 5). 11 experimental runs indicate a piecewise linear decrease in torque with decreasing pressure, starting from $0.4\,\text{Nm}$ at $58\,\text{kPa}$ gauge pressure to $0\,\text{Nm}$ at $4\,\text{kPa}$. The modeled torque of both models is

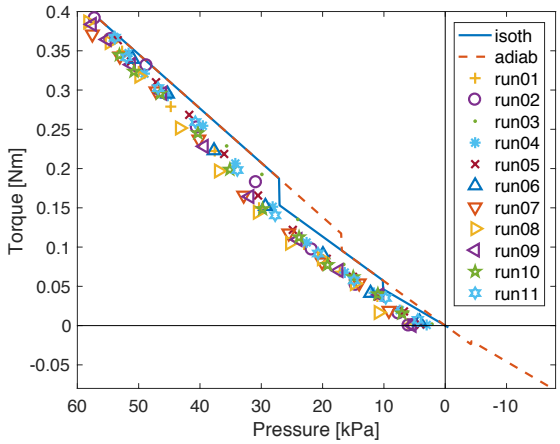

Fig. 6: Joint extending torque τ as function of pressure; experimental data (marker points) and isothermal and adiabatic modeled data (solid and broken line) from the static characterization experiment. The x-axis is horizontally flipped, for reading convenience: chamber pressure drops and reduces joint torque. Data points are experimental recordings of 11 static experimental measurements. Torques under $0\,\mathrm{Nm}$ are not possible in this joint design, the pressure bag only produces positive forces. Theoretical, negative torque values for the adiabatic model are shown to visualize the model behaviour.

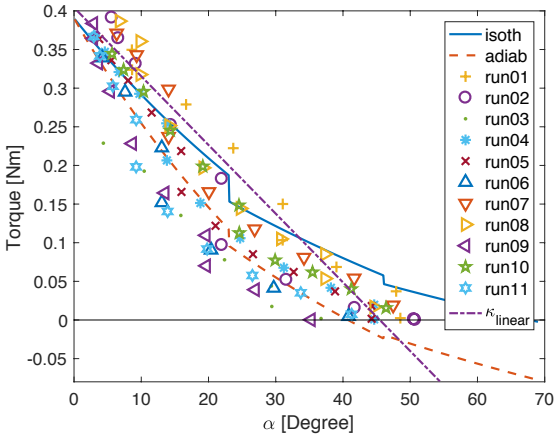

Fig. 7: Joint extending torque τ as function of working angle α. Experimentally recorded data (markers) is identical to Fig. 6, α was extracted from video data. Overlaid solid and broken lines show the modeled angle-torque relationship under the assumption of an isothermal or adiabatic model, respectively. The violet line shows a linear α/τ model.

slightly higher than the measured values. The experimental torque-angle relationship (Fig. 7) also follows both models, experimental data lies roughly between both models. The experimentally measured joint torque drops to zero between $\alpha = 35°$ and $\alpha = 50°$. We added a hypothetical, simple linear joint torque model in Fig. 7. Its stiffness κ_{linear} roughly matches the global, linear stiffness of the experimental data with peak torque $\tau_{\mathrm{lin,peak}} = 0.4\,\mathrm{Nm}$ and a zero crossing at $\alpha = 45°$. The torque-angle relationship for a linear joint stiffness is therefore $\tau_{\kappa\mathrm{linear}}(\alpha) = -0.509\alpha + 0.4$. Plots in Fig. 7 and Fig. 8 emphasize the difference between nonlinear joint torque generation through spring relaxation with air as pressure medium (isothermal or adiabatic model) and a stepwise change of pressure volume and working area, versus a hypothetical, linear torque-angle relationship.

Modeled Jumping Height: We established an isothermal, adiabatic and a linear model for the joint torque-angle relationship (Fig. 7). During joint release movement, the spider-inspired leg joint produces positive work equivalent to the covered area under the torque-angle curve. For a simplified estimation of the maximum jumping height we assume that all energy released converts into potential energy, i.e. maximum jumping height of the robot:

$$E(\alpha) = \int_{\alpha_1}^{\alpha_2} \tau(\alpha) d\alpha = E_{\mathrm{pot}} = mgh(\alpha) \tag{6}$$

$$h(\alpha) = \int_{\alpha_1}^{\alpha_2} \tau(\alpha) d\alpha \cdot \frac{1}{mg} \tag{7}$$

Model predictions of jumping height are visualized in Fig. 8. Positive work done by the joint follows the release direction of a virtual spring, leading to a jumping height characteristics following the shape of an inverted parabola shape, until peak height. The isothermal model predicts a maximum jumping height of $46\,\mathrm{cm}$ at $69°$, the adiabatic model $31\,\mathrm{cm}$ at $40°$. The simple linear model predicts a maximum jumping height of $45\,\mathrm{cm}$ at $45°$. It should be noted that an increase of working angle α beyond reaching peak height (model zero-crossings in Fig. 7) does not lead to negative work, as the applied pressure bag is only acting in one direction, and never flexes the leg joint.

Experimental Jumping Height: Working angle α in the jumping experiment was extracted from high-speed recordings during the first $15\,\mathrm{ms}$ to $20\,\mathrm{ms}$ until lift-off, as range of joint rotation while in contact with the ground (Fig. 9). The extracted lift-off working angle of 23 recorded jumps varied between $16°$ and $47°$ (Fig. 8). Jumping height varied between $5\,\mathrm{cm}$ at $16°$, and $11.5\,\mathrm{cm}$ at $45°$. A typical jump off sequence starting from joint release until leaving ground took $20\,\mathrm{ms}$, and a full jump lasted around $200\,\mathrm{ms}$, until landing (Fig. 9)[1].

V. Discussion

We presented a novel, scalable pneumatic and tendon driven robotic joint with a design inspired by the hydraulic and muscle driven joints of spider legs.

Jumping experiments and possible sources of error: The maximum, experimental jumping height reached was $11.5\,\mathrm{cm}$, corresponding to i.e. $37\,\%$ of the modeled, adiabatic jumping height. Due to the fast expansion of the joint we make the assumption that this experimental case is closer to the described adiabatic model, instead of the isothermal model. A precise validation of either the isothermal or the adiabatic model assumption is hard, and would likely require monitoring the instantaneous air chamber temperature. Our simplification of full work conversion into jumping height disregards several possible energetic losses: rotational movements, losses due to elasticities and sliding, drag losses from attached cables and the pressure hose, and friction losses. Model parameters

[1]Video at `https://youtu.be/xfP-7sbfiWk?t=157`

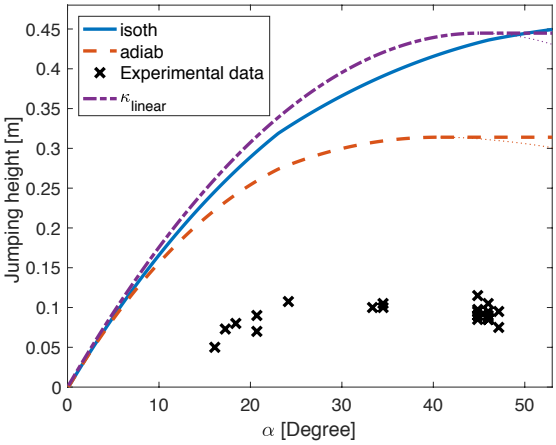

Fig. 8: Jumping height depending on lift-off working angle α, which is the swept joint angle during ground contact. Continuous line: modeled jumping based on a linearised rotational joint stiffness κ_{linear}. Individual data markers are extracted experimental jumping heights from 23 high speed video camera recordings of dynamic jumps.

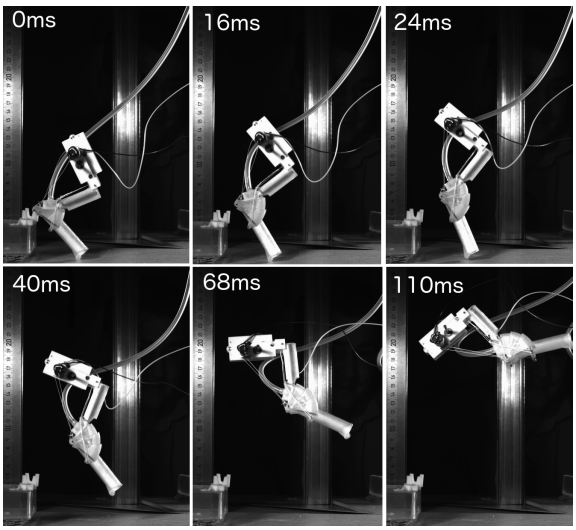

Fig. 9: Snapshot series of a dynamic jump of the spider inspired leg-joint. Lift-off is reached after 17 ms, apex height after 110 ms. A flex-hold-release mechanism initially flexes the leg joint through a cable. The spider-inspired actuator joint is then pressurized by an external miniature air pump to 58 kPa gauge pressure. The tensioning motor is reversed, releasing the joint at $t = 0$ ms. The pressurized chamber acts as an air-spring, rapidly extends the leg joint, and catapults the robot leg in this example 11.5 cm upwards.

were estimated based on CAD extracted values which might differ in hardware. Measured values of soft elements might change under pressure, such as the radius of connection tubes. Furthermore, for some jumping experiments the air pressure opened the joint before release (less than 10°) and the starting angle deviated accordingly.

Shell structure and pressure bag: The spider-inspired joint mechanism implemented from shell elements allows a working angle up to 69°. The adiabatic model predicts that around 40° would be utilized before reaching outside pressure. To provide more extended application of positive joint work measures to compensate for potential adiabatic pressure losses would be required. Torque losses experienced through the finite shell thickness are visible in the isothermal-modeled torque-angle characteristics as vertical steps in Fig. 7, and amount to 0.05 Nm (13 % of 0.4 Nm). An improved design would apply shell elements as thin as possible. Our torque-angle measurements and the corresponding adiabatic model show not a linear but reasonably good torque-angle characteristic leading to a relatively efficient leg actuation. We think that with further design improvements and especially a change in actuation medium (i.e. hydraulics), the spider-inspired leg joint design could compete with piston actuated leg joints which require a carefully placed piston, and have an overall more restricted working range [24]. A drawback of our proposed system is its double-membrane design composed of shell elements and internal pressure bag. Assumed friction between shell elements and the inner bag leads to a reduced jumping height. Low friction materials or a single-membrane design could reduce such losses.

Actuation mechanism and medium: The spider-inspired joint actuation mechanism includes a pneumatic extension mechanism and a flex-hold-release system inspired by Dash robot's clutch mechanism [23]. The leg including the release mechanism weighs 36 g. Currently, its pressure pump and power source are not placed onboard, and are not included in the weight calculation. Small battery solutions i.e. for micro gliders exist, and onboard miniature pumps in the gram range could replace the 14 g heavy external pump. An important experimental component was a robust and rapidly acting flex-hold-release mechanism. Our implementation could withstand up to tested 0.45 Nm joint torque, and released within a few milliseconds. The internal bag is reusable and lasted more than 100 experimental runs for a tested gauge pressure up to 58 kPa. Spiders with a size range from a few millimeters to several centimeters apply a similar geometric actuator design as our mechanical implementation. Our model indicates that rotatory fluidic extensor systems like the presented mechanism torque-scale well with increasing size, with the cost of a larger pressurized volume depending quadratically on the radius of the pressure chamber. Here, we applied air pressure as actuator medium. However, the comparison between the isothermal and the adiabatic model shows that a 30 % loss in (modeled) jumping height is due to the adiabatic pressure loss at rapid volume expansion. Spiders applying haemolymph as actuator medium potentially avoid such losses.

VI. Conclusion and Future Work

We presented the design of a compact, 36 g lightweight, spider-inspired, fluidic air pressure and electrically actuated leg joint mechanism. It jumps 11.5 cm in 110 ms at 58 kPa chamber pressure, from a initial hip height of 10 cm. We modeled its torque-angle and torque-pressure characteristics and jumping height based on three models: isothermal, adiabatic, and linear. We compared experimentally, statically obtained torque-angle and torque-pressure recordings, and

dynamic jumping experiments to our model predictions.

The major and novel design component of the presented system is a fluid-actuated, rotational leg joint with *a)* a perpendicular contact angle between the active pressure area and the actuator's shell elements, and *b)* an arc-shape, nested shell structure. This design effectively transfers all energy from pressure to joint torque as the leg unfolds, and mimics the observable morphology in spider leg joints. A custom-designed, low friction bag seals the shape-changing actuator. Torque-pressure characteristics of the joint show reach up to $0.4\,\mathrm{Nm}$ torque at a pressure of $58\,\mathrm{kPa}$, at a chamber radius less than $27\,\mathrm{mm}$.

By electrically actuating a flex-hold-release mechanism connected via a joint-flexing tendon, the robotic leg is flexed, then charged with air pressure, and rapidly released. Vertical jumps catapulted the robot vertically $11.5\,\mathrm{cm}$ into the air. The adiabatic model predicts that 3 times higher vertical jumps should be feasible, with improvements to the mechanism to avoid losses.

While details about the exact morphology and functional biomechanics of pressure extended joints in spiders are not yet available, our physical and simulation models starts shedding light at several aspects. We assume that our two-layered shell-membrane design is relatively strong-damped for high speed movements, which causes losses in jumping height. Spider joints likely feature a more sophisticated membrane design to decrease damping at rapid movements and high loads. Further, to produce high joint torque for dynamic jumps we pressurized air inside shell segments and the connected reservoir. Spiders use incompressible haemolymph fluid to actuate leg joints, and potentially feature other mechanisms to elastically store energy.

Although the joint mechanism presented here is able to extend with very little parasitic torque especially at slow speeds, it might be worth sacrificing optimality for a simpler mechanism. In future work, we also plan to examine joints connected by soft membranes, i.e. fiber-reinforced flexible actuators [25]. Such designs could offer advantages such as: inexpensive, easy, and rapid manufacturing, low wear, lightweight, and inherent ability to seal fluids. We are also interested in the size scaling characteristics of spider-inspired torque actuators, i.e. by implementing a complete system in the small centimeter range. Physics in small and narrow volumes changes, and a miniature hardware model could contribute to the understanding of fluid actuator characteristics in spider leg joints.

VII. Acknowledgments

We thank the MPI Department Spatz for allowing us to use the SEM equipment. We further thank our anonymous reviewers for constructive comments and helpful suggestions.

References

[1] P. Jaeger, "A new species of Heteropoda (Araneae, Sparassidae, Heteropodinae) from Laos, the largest huntsman spider?" *Zoosystema*, vol. 23, no. 3, pp. 461–465, 2001.

[2] C. Kropf, "Hydraulic system of locomotion," in *Spider Ecophysiology*. Springer, 2013, pp. 43–56.

[3] S. Reußenzehn, "Mechanical design of the legs of Dolomedes aquaticus-Novel approaches to quantify the hydraulic contribution to joint movement and to create a segmented 3D spider model," Ph.D. dissertation, University of Otago, 2010.

[4] W. Neubauer, "A spider-like robot that climbs vertically in ducts or pipes," in *IROS'94 proceedings*, vol. 2. IEEE, 1994, pp. 1178–1185.

[5] C. Menon, Y. Li, D. Sameoto, and C. Martens, "Abigaille-I: towards the development of a spider-inspired climbing robot for space use," in *2008 2nd IEEE RAS & EMBS International Conference on Biomedical Robotics and Biomechatronics*. IEEE, 2008, pp. 384–389.

[6] R. Blickhan and F. G. Barth, "Strains in the exoskeleton of spiders," *Journal of Comparative Physiology A*, vol. 157, no. 1, pp. 115–147, 1985.

[7] D. Parry, "Spider leg-muscles and the autotomy mechanism," *Journal of Cell Science*, vol. 3, no. 43, pp. 331–340, 1957.

[8] J. Anderson and K. Prestwich, "The fluid pressure pumps of spiders (Chelicerata, Araneae)," *Zeitschrift für Morphologie der Tiere*, vol. 81, no. 4, pp. 257–277, 1975.

[9] R. Wilson, "Some comments on the hydrostatic system of spiders (Chelicerata, Araneae)," *Zeitschrift für Morphologie der Tiere*, vol. 68, no. 4, pp. 308–322, 1970.

[10] T. Weihmann, M. Günther, and R. Blickhan, "Hydraulic leg extension is not necessarily the main drive in large spiders," *Journal of Experimental Biology*, vol. 215, no. 4, pp. 578–583, 2012.

[11] T. Weihmann, M. Karner, R. J. Full, and R. Blickhan, "Jumping kinematics in the wandering spider Cupiennius salei," *Journal of Comparative Physiology A*, vol. 196, no. 6, pp. 421–438, 2010.

[12] L. Zentner, "Modelling and application of the hydraulic spider leg mechanism," in *Spider Ecophysiology*. Springer, 2013, pp. 451–462.

[13] M. Schwörer, M. Kohl, and W. Menz, "Fluidic microjoints based on spider legs," in *Conf. on New Actuators (Bremen)*, 1998.

[14] C. Menon and C. Lira, "Active articulation for future space applications inspired by the hydraulic system of spiders," *Bioinspiration & biomimetics*, vol. 1, no. 2, p. 52, 2006.

[15] I. Gaiser, S. Schulz, H. Breitwieser, and G. Bretthauer, "Enhanced flexible fluidic actuators for biologically inspired lightweight robots with inherent compliance," in *Robotics and Biomimetics (ROBIO), 2010 IEEE International Conference on*. IEEE, 2010, pp. 1423–1428.

[16] J. Berring, K. Kianfar, C. Lira, C. Menon, and F. Scarpa, "A smart hydraulic joint for future implementation in robotic structures," *Robotica*, vol. 28, no. 07, pp. 1045–1056, 2010.

[17] H. Faraji, R. Tachella, and R. L. Hatton, "Aiming and vaulting: Spider inspired leaping for jumping robots," in *2016 IEEE International Conference on Robotics and Automation (ICRA)*. IEEE, 2016, pp. 2082–2087.

[18] M. Kovac, M. Schlegel, J.-C. Zufferey, and D. Floreano, "A miniature jumping robot with self-recovery capabilities," in *2009 IEEE/RSJ International Conference on Intelligent Robots and Systems*. IEEE, 2009, pp. 583–588.

[19] M. A. Woodward and M. Sitti, "Multimo-bat: A biologically inspired integrated jumping–gliding robot," *The International Journal of Robotics Research*, vol. 33, no. 12, pp. 1511–1529, 2014.

[20] T. Tanaka and S. Hirose, "Development of leg-wheel hybrid quadruped airhopper design of powerful light-weight leg with wheel," in *2008 IEEE/RSJ International Conference on Intelligent Robots and Systems*. IEEE, 2008, pp. 3890–3895.

[21] R. F. Shepherd, A. A. Stokes, J. Freake, J. Barber, P. W. Snyder, A. D. Mazzeo, L. Cademartiri, S. A. Morin, and G. M. Whitesides, "Using explosions to power a soft robot," *Angewandte Chemie International Edition*, vol. 52, no. 10, pp. 2892–2896, 2013.

[22] B. Shin, H.-Y. Kim, and K.-J. Cho, "Towards a biologically inspired small-scale water jumping robot," in *2008 2nd IEEE RAS & EMBS International Conference on Biomedical Robotics and Biomechatronics*. IEEE, 2008, pp. 127–131.

[23] G. P. Jung, C. S. Casarez, S. P. Jung, R. S. Fearing, and K. J. Cho, "An integrated jumping-crawling robot using height-adjustable jumping module," in *2016 IEEE International Conference on Robotics and Automation (ICRA)*, May 2016, pp. 4680–4685.

[24] C. Semini, "HyQ - Design and Development of a Hydraulically Actuated Quadruped Robot," Ph.D. dissertation, IIT, Italy, 2010.

[25] K. C. Galloway, P. Polygerinos, C. J. Walsh, and R. J. Wood, "Mechanically programmable bend radius for fiber-reinforced soft actuators," in *Advanced Robotics (ICAR), 2013 16th International Conference on*. IEEE, 2013, pp. 1–6.